

Highly Efficient Red Quantum Dot Light-Emitting Diodes by Balancing Charge Injection and Transport

Yunfeng Fang, Penglong Bai, Jiayi Li, Binbin Xiao, Yiqing Wang, and Yanping Wang*



Cite This: *ACS Appl. Mater. Interfaces* 2022, 14, 21263–21269



Read Online

ACCESS |

Metrics & More

Article Recommendations

ABSTRACT: Quantum dot light-emitting diodes (QLEDs) have promising commercial value and application prospects in the fields of displays and lighting. However, a charge-transfer imbalance always exists in the devices. In this work, the high-efficiency red QLEDs were obtained via employing the mixtures of poly[(9,9-diptylfluorenyl-2,7-diyl)-alt-(4,4'-(N-(4-butylphenyl)) (TFB) and 4,4'-bis(carbazole-9-yl)-1,1'-biphenyl (CBP) as hole-transport layers (HTLs) by solution processing. The optimized mixing concentration of CBP is 20 wt %. The corresponding red QLED exhibited a maximum luminance of 963 433 cd m⁻², a maximum current efficiency of 38.7 cd A⁻¹, an external quantum efficiency of 30.0%, a central wavelength of 628 nm with a narrow full width at half-maximum (fwhm) of 24 nm, and a 5-fold T_{50} lifetime enhancement at an extremely high luminance of 200 000 cd m⁻². The characteristics of carrier-only devices with QD emissive layers (QD EMLs) and impedance characteristics of QLEDs demonstrate that these advances are chiefly ascribed to the more balanced charge transport and efficient hole–electron recombination in EML. We anticipate that our results could offer a low-cost and simple solution-processed method for preparing high-performance QLEDs.

KEYWORDS: quantum dot light-emitting diodes, high-efficiency, charge injection and transport, charge balance, device stability

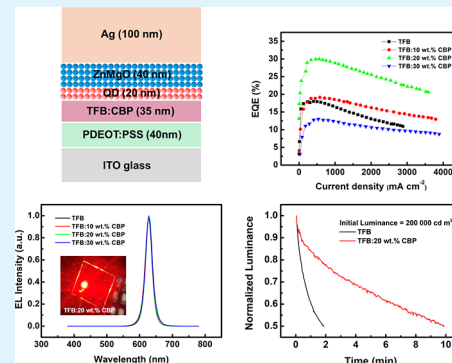
INTRODUCTION

Over the past few decades, quantum dot light-emitting diodes (QLEDs) have drawn tremendous attention as ideal candidates for new-generation solid-state lighting and display technologies because of their outstanding merits such as high color saturation, facile color tunability, and easy solution process.^{1–10} The working principle of QLED is that under the action of an external driving voltage, holes and electrons are injected into the quantum dot emissive layer (QD EML) through the hole-transport layer (HTL) and electron-transport layer (ETL) from the anode and cathode, respectively, accompanied by radiative recombination and photon emission. Therefore, the device performance significantly depends on the carrier recombination. This requires holes and electrons to be injected quickly and equally into the QD EML.¹¹

Generally, most QLEDs based on a hybrid architecture consist of organic HTL and metal oxide nanoparticle-based ETL. It is well-known that the hole mobilities of most organic HTLs are much lower than the electron mobilities of the ETLs. This leads to imbalanced injection of holes and electrons, which easily charges the QD EMLs in QLEDs.¹² In this case, Auger recombination occurs where the holes and electrons recombine and release energy, which excites electrons in the conduction band to a higher energy level without emitting photons.¹³ These excited electrons rapidly thermalize back to their ground state and lose the energy in the

form of heat,¹⁴ which reduces the light emission from QD EMLs. The excess electrons could overflow¹⁵ and eventually be collected by the anode, forming the leakage current and producing the Joule heat. In addition, accelerated Förster resonance energy transfer via the charge accumulation and the formation of leakage current induced by excess electrons greatly quenches the light emission and thus deteriorates the device efficiency.^{16,17}

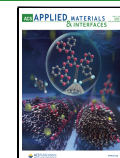
As a result, addressing the problem of imbalanced charge injection and transport in QLEDs is urgently needed. Much effort has been made to address it, generally including two aspects. One is to impede the excess electrons from injecting into the QD EML through modifying the ETL, such as size and surface modification,^{18,19} or introducing a thin insulating polymer or metal oxide between the ETL and the QD EML.^{20,21} Dopants such as Mg,^{22,23} Al,²⁴ Li,²⁵ polyethylenimine (PEI),²⁶ polyvinylpyrrolidone (PVP),²⁷ and polyethylenimine ethoxylated (PEIE)²⁸ can also be added to ZnO to elevate its conduction band minimum and decrease its electron



Received: March 10, 2022

Accepted: April 21, 2022

Published: April 29, 2022



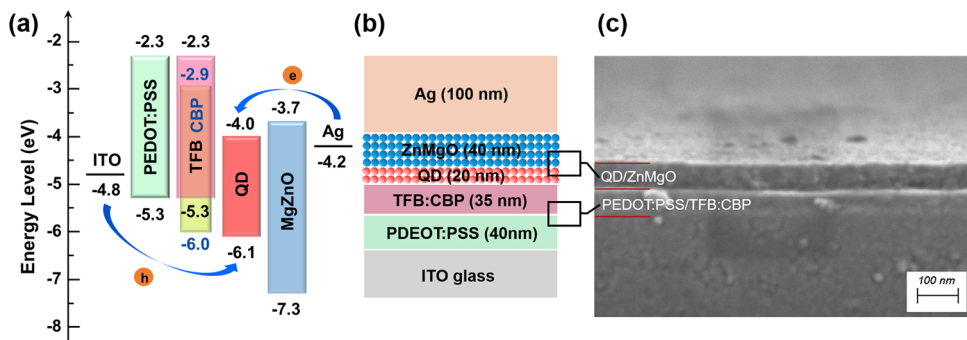


Figure 1. (a) Energy level alignment of each material of red QLEDs. (b) Device configuration of red QLEDs. (c) Cross-section of a representative device.

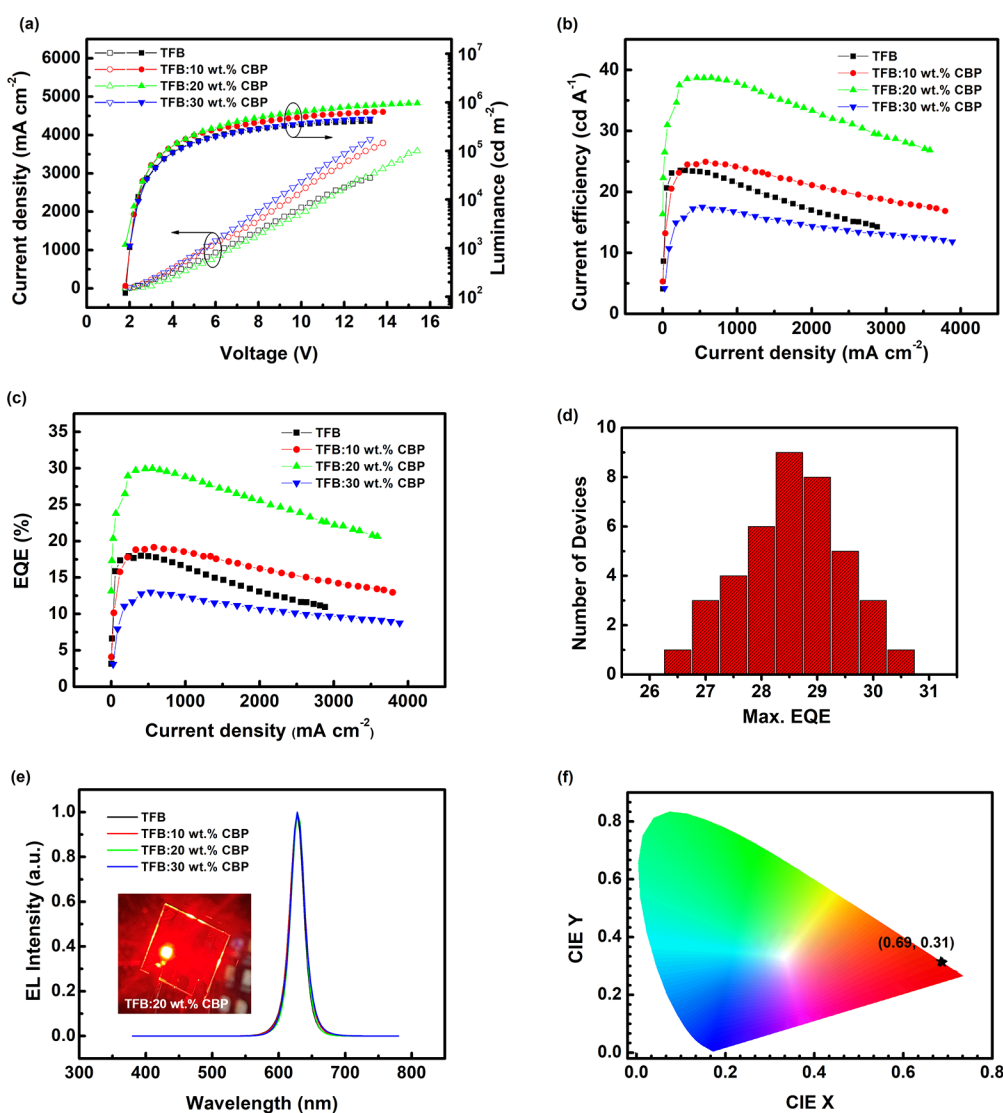


Figure 2. Device performance of the developed QLEDs. (a) Current density–voltage–luminance (J – V – L) characteristics. (b) Current efficiency vs current density characteristics. (c) External quantum efficiency vs current density characteristics. (d) Histogram of maximum EQE measured from 40 devices ($x = 20 \text{ wt\%}$). (e) Normalized EL spectra at $\sim 1000 \text{ cd m}^{-2}$ (Inset: lighting on image of QLEDs with TFB:20 wt % CBP as HTL at an operation voltage of 2 V). (f) CIE coordinates of the corresponding red QLEDs with different HTLs.

mobility. The other is to promote the hole injection by optimizing the HTLs, for instance, the mixed small molecule HTL,²⁹ employing polymer and small molecule mixtures as HTLs,³⁰ or raising the shell conduction band edge of QDs by the composition tailoring.^{31,32} In addition, some works

presented stepwise polymer/polymer co-HTLs such as poly-[bis(4-phenyl)(4-butylphenyl)amine] (poly-TPD)/poly(9-vinylcarbazole) (PVK)^{33,34} and poly[(9,9-diethylfluorenyl-2,7-diyl)-alt-(4,40-(N-(4-butylphenyl))]^{35,36} (TFB)/PVK. Under this condition, solvent erosion and intermixing need to be

addressed, and adding a layer complicates the preparation process. However, there are still some challenges to be overcome at the current stage, such as solvent erosion in the solution processing of multilayered devices, charge carrier injection and transport imbalance, and rapid efficiency roll-off.

A few HTL materials have high hole mobilities, such as TFB,^{37–39} which is as high as $1 \times 10^{-2} \text{ cm}^2 \text{ V}^{-1} \text{ s}^{-1}$. Apparently, it can also cause an imbalance in hole and electron transport. 4,4'-Bis(carbazole-9-yl)-1,1'-biphenyl (CBP)⁴⁰ presents a relatively low hole mobility of $1 \times 10^{-4} \sim 10^{-3} \text{ cm}^2 \text{ V}^{-1} \text{ s}^{-1}$ and a deep highest occupied molecular orbital (HOMO) energy level of -6.0 eV . In this work, we selected TFB mixed CBP as HTLs because it can realize efficient hole injection between HTL and QD EML. Herein, the excellent-performance red QLEDs exhibit a maximum luminance of 963 433 cd m⁻², a maximum EQE of 30.0% and a maximum current efficiency of 38.7 cd A⁻¹. We carefully investigated the influence of CBP on the device characteristics and found that the improvement in device performance was attributed to the more balanced hole and electron transport in QD EML.

RESULTS AND DISCUSSION

The schematic energy diagrams of different materials in the red QLEDs, the device structure, and the cross section of a typical device are shown in Figure 1a–c. The characteristic values of the HOMO, lowest unoccupied molecular orbital (LUMO), valence and conduction edges were reported by others.^{39–41} Obviously, holes and electrons can be efficiently injected into QD EML from HTL and ETL, respectively. The HOMO values of PEDOT:PSS and TFB are equal to -5.2 and -5.3 eV , respectively, leading to the efficient hole injection from PEDOT:PSS to TFB. However, to some extent, the introduction of CBP in HTL increases the energy barrier between these two layers, which limits the hole injection. The energy diagram from Figure 1a provides an important guideline for the selection of materials, which does not provide sufficient information on the mixing concentration of CBP. To optimize the device structure, we need to balance the concentrations of holes and electrons in the QD EML. Therefore, we optimized the mixing concentration of CBP from 0 to 30 wt %. The SEM cross-sectional image of a typical device is presented in Figure 1c. The thicknesses of the PEDOT:PSS/TFB:CBP and QD/ZnMgO are estimated to be 75 and 60 nm, respectively.

Figure 2 illustrates the corresponding current density–voltage-luminance ($J-V-L$), current efficiency–current density (CE– J), and external quantum efficiency–current density (EQE– J) characteristics and normalized EL spectra of QLEDs with different x . From Figure 2a, it is clear that the luminance of the QLED at $x = 20 \text{ wt } \%$ reaches as high as 963 433 cd m⁻², which is more than two times higher than that of the device at $x = 0$ (pure TFB HTL). It can be seen from panels b and c of Figure 2 that the CE and EQE of QLED at $x = 20 \text{ wt } \%$ are higher than those of the other three devices, indicating much more balanced concentrations of holes and electrons in QD EML. The best device performance is achieved with the maximum efficiencies reaching up to 38.7 cd A⁻¹ for CE and 30.0% for EQE, respectively. As can be clearly seen from Figure 2d, the histogram of the maximum EQE for 40 devices presents the EQE varying in the range of 26.5–30.5% with a mean of 28.5% and a standard deviation of 8%, indicating excellent device reproducibility. In contrast to QLED based on TFB as HTL, the CE and EQE at $x = 20 \text{ wt } \%$ are remarkably

enhanced by approximately 65 and 67%. Even at a high luminance of 100 000 cd m⁻², the CE and EQE still remain at 37.5 cd A⁻¹ and 28.9%, respectively, as listed in Table 1. The

Table 1. Performance Summary of QLEDs with Different HTLs

device	V_{on}^a (V)	L_{max} (cd m ⁻²)	CE ^b (cd A ⁻¹)	EQE ^b (%)
TFB	1.8	410 659	23.5, 23.5, 23.3	18.0, 17.9, 17.9
TFB:10 wt % CBP	1.8	639 041	24.9, 23.1, 24.5	19.1, 17.8, 18.9
TFB:20 wt % CBP	1.8	963 433	38.7, 30.9, 37.5	30.0, 23.8, 28.9
TFB:30 wt % CBP	2.0	459 459	17.5, 16.7, 17.1	12.9, 12.3, 12.7

^aDefined as the applied voltage when the luminance is detected by the luminance meter. ^bThe three numbers in each entry represent the maximal CE and EQE, the CE and EQE at a luminance of 50 000 cd m⁻², and the CE and EQE at a luminance of 100 000 cd m⁻², respectively.

QLED at $x = 30 \text{ wt } \%$ exhibits the poorest performance, which may be contributed to the severe unbalanced carriers transport in the device. Figure 2e displays the normalized EL spectra of these four devices and photo of QLED at $x = 20 \text{ wt } \%$ operated at 2 V. The higher luminance and uniform emission can be observed in the photo. All the devices display a central wavelength of 628 nm, with a full width at half-maximum (fwhm) of 24 nm corresponds to Commission International de l'Eclairage (CIE) color coordinates of (0.69, 0.31), as shown in Figure 2f. The detailed performance parameters are listed in Table 1.

To understand the observed performance difference, we fabricated the HODs with different x to compare with the EOD. It was reported that the electron mobility of ZnMgO was reported as $\sim 1 \times 10^{-3} \text{ cm}^2 \text{ V}^{-1} \text{ s}^{-1}$.⁴² The current–voltage ($I-V$) curves of HODs and EOD are depicted in Figure 3.

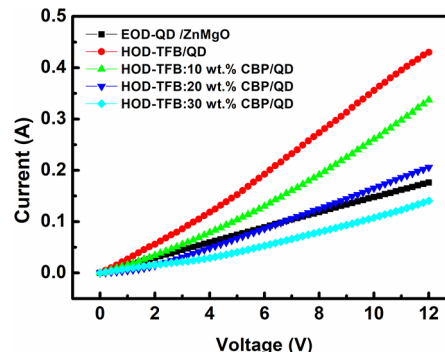


Figure 3. Current versus voltage ($I-V$) plots of HODs with QD layers based on different HTLs and the EOD with QD layer.

Clearly, the current density of HOD with pure TFB is higher than that of EOD at the same voltage. As the mixing concentration of CBP is increased, the current gradually decreases. As analyzed above, when $x = 20 \text{ wt } \%$, the concentrations of holes and electrons in the QD EML are much balanced. The current of EOD exceeds that of HOD as x reaches to 30 wt %, revealing that excessive CBP impedes the hole transport.

According to the literature reports, impedance spectroscopy monitors the system response to AC modulation. The data can be used to reveal charge transfer and recombination processes.^{43–45} Hence, impedance spectroscopy was employed to detect the processes in red QLEDs. Figure 4 shows the

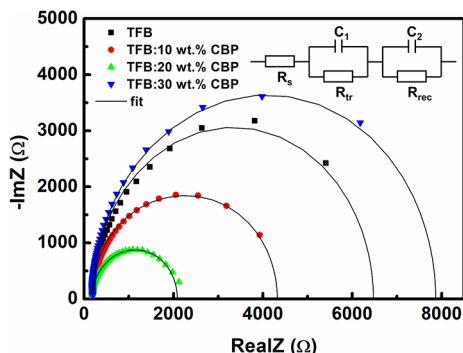


Figure 4. Cole–Cole plots of red QLEDs with different HTLs at a forward bias of 4.0 V (inset: equivalent circuit).

Cole–Cole plots of QLEDs with different x at 4.0 V, which can be modeled by a two-blocked electrical equivalent circuit network. The recombination resistance (R_{rec}) is defined as the reverse derivative of voltage as a function of the recombination current. The hole–electron recombination probability is then reversely proportional to R_{rec} .⁴⁶ It was found that the two-blocked circuit fitted experimental data very well. The R_{rec} is estimated to be 4080, 2658, 1221, and 5404 Ω for pure TFB, $x = 10$, 20, and 30 wt %, respectively. Consequently, the sequence of the hole–electron recombination rate in these four QLEDs from high to low is $x = 20$ wt %, $x = 10$ wt %, pure TFB, and $x = 30$ wt %, which is in good agreement with the above discussion. That is, the device with $x = 20$ wt % has the highest hole–electron recombination rate.

To further explore the different performance when x has various values, we employed atomic force microscopy (AFM) to examine the surface morphologies of ITO/PEDOT:PSS/HTLs, as illustrated in Figure 5. The root-mean-square (RMS) values of HTLs with pure TFB, $x = 10$, 20, and 30 wt % are 0.6899, 0.7012, 0.7209, and 0.7368 nm, respectively, which demonstrates that the RMS increases as x is increased. It means the hole transport is hindered to a certain degree. the RMS of the interface morphology is the smallest for the pure TFB film, and it has the strongest hole-transport capability.

In addition, it is known that energy levels and corresponding energy barriers influence the charge injection and transport. Therefore, the energy levels of pure TFB and each mixed HTL were tested using ultraviolet photoelectron spectroscopy (UPS), as depicted in Figure 6. The onset energy (E_{onset}) of TFB, $x = 10$, 20, and 30 wt % HTLs are determined as 1.02, 1.09, 1.13, and 1.14 eV, respectively, which means the HOMO energy level shifts from 1.02 to 1.14 eV relative to the Fermi level. The corresponding work functions (W_F) are about 4.31, 4.36, 4.34, and 4.34 eV, respectively. The HOMO level of these HTLs can then be calculated as 5.33, 5.45, 5.47, and 5.47 eV according to the equation $\text{HOMO} = E_{\text{onset}} + W_F$, suggesting a little harder hole-injecting at the interface of the PEDOT:PSS/TFB:CBP when compared with the interface of PEDOT:PSS/TFB. On the basis of the above analysis, it can be concluded that the main factor affecting the hole transport is the hole mobilities of TFB and CBP.

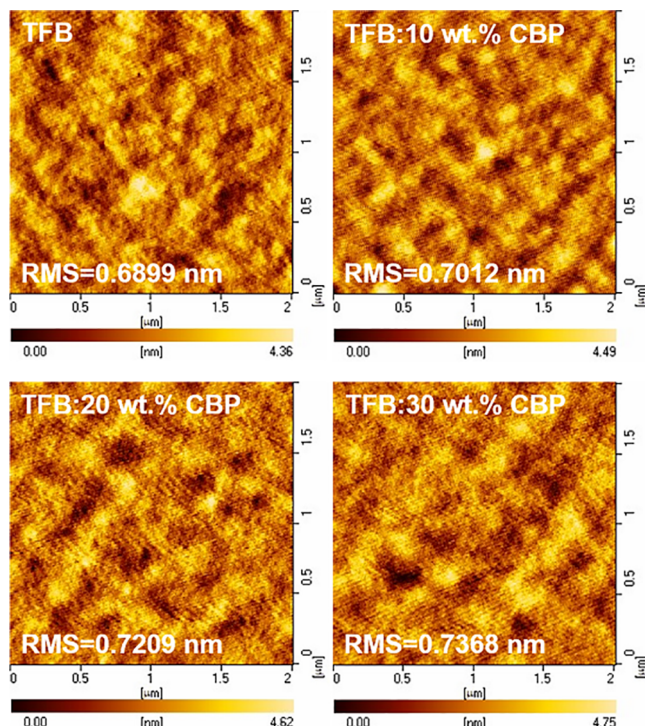


Figure 5. AFM images and surface roughness RMS values for different HTLs.

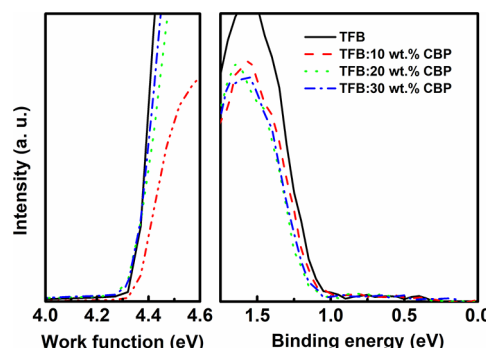


Figure 6. UPS spectra of pure TFB and each mixed HTL. Left: the work function region showing the secondary electron cutoff. Right: valence band region near the Fermi energy.

Stability tests for QLEDs based on TFB and TFB:20 wt % CBP as HTLs, respectively, were conducted at an initial luminance of $\sim 200\,000 \text{ cd m}^{-2}$. As shown in Figure 7, the T_{50}

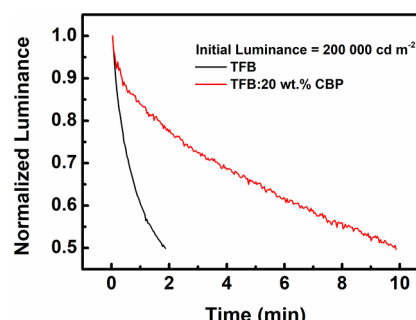


Figure 7. Device stability at an initial luminance of about $200\,000 \text{ cd m}^{-2}$ for TFB and TFB:20 wt % CBP as HTLs, respectively.

lifetimes of these two devices are determined to be 2 and 10 min, respectively. At such high luminance, the T_{50} lifetime of the QLED with TFB:20 wt % CBP as the HTL is indeed five times longer than that of the QLED with pure TFB as the HTL. These results reveal that the relatively balanced carrier transport is the main factor in the improvement of device performance in this work.

CONCLUSIONS

In summary, we demonstrate well-optimized red QLEDs based on TFB: (x) CBP as HTLs through solution-processed technology. As $x = 20$ wt %, the corresponding QLED expresses a maximal luminance of 963 433 cd m⁻², a maximal CE of 38.7 cd A⁻¹ and a maximal EQE of 30.0% and a narrow fwhm (24 nm). Our devices maintain a CE of 37.5 cd A⁻¹ and EQE of 28.9% at a high luminance of 100 000 cd m⁻², respectively. On the basis of the experimental results, it can be concluded that the relative balance of hole and electron transport in QLEDs is achieved by introducing appropriate concentrations of CBP into TFB as the HTL and then enhancing the device performance. This work offers an effective route to obtain high-efficiency QLEDs, and we hope it can accelerate the applications of cost-effective and large-area displays via solution processing.

EXPERIMENTAL SECTION

Materials. PEDOT:PSS Clevios AI 4083 (poly(ethylenedioxythiophene):polystyrenesulfonate was purchased from Heraeus Electronic Materials Division. TFB and CBP were purchased from Xi'an Polymer Light Technology Corp. (PLT). ZnMgO nanoparticles in ethanol solution and red QDs solution with CdZnSe/CdZnS/ZnS core/shell structure ($QY \approx 96\%$) were purchased from Mesolight Inc. Ethanol, methylene chloride, acetone, octane, and isopropanol were purchased from Sigma-Aldrich.

Device Fabrication. The ITO glass substrates were cleaned as described previously.⁴⁷ Red QLEDs with a configuration of ITO/PEDOT:PSS (40 nm)/TFB:CBP (x, 35 nm)/QDs (20 nm)/ZnMgO (40 nm)/Ag (100 nm) were fabricated on the cleaned ITO substrates. The mixing concentration x was varied as 0, 10, 20, and 30 wt %. The TFB:CBP layers (in chlorobenzene, 6 mg mL⁻¹) were coated at 3000 rpm for 40 s and baked at 110 °C for 10 min. Other functional layers and hole- and electron-only devices with QD layers (HOD and EOD) were prepared as reported in ref 47. The structures of HOD and EOD were ITO/PEDOT:PSS (40 nm)/TFB:CBP (x, 35 nm)/QD (20 nm)/Ag and ITO/QD (20 nm)/ZnMgO (40 nm)/Ag, respectively. The device area was 2 mm × 2 mm as defined by the overlapping area of the ITO and the Ag electrode.

Characterization. The current–voltage (I – V) characteristics of hole- and electron-only devices, the current density–voltage–luminance (J – V – L) characteristics and EL spectra of red QLEDs, the complex impedance measurements of the sensors, the surface morphologies of the HTLs on ITO/PEDOT:PSS substrates, and ultraviolet photoelectron spectroscopy (UPS) measurements were conducted using the apparatus described in ref 47. EQEs were calculated from the luminance, current density, and EL spectra, assuming a Lambertian distribution. Scanning electron microscopy (SEM, ZEISS Sigma 300) was used to obtain the cross-sectional images of QLEDs. All the measurements were carried out at room temperature.

AUTHOR INFORMATION

Corresponding Author

Yanping Wang – School of Materials Science and Engineering, Changchun University of Science and Technology, Changchun 130022, People's Republic of China;  orcid.org/0000-

0002-2344-366X; Phone: +86 431 85583188;
Email: ypwang2015@163.com; Fax: + 86 431 85583188

Authors

Yunfeng Fang – School of Materials Science and Engineering, Changchun University of Science and Technology, Changchun 130022, People's Republic of China
Penglong Bai – School of Materials Science and Engineering, Changchun University of Science and Technology, Changchun 130022, People's Republic of China
Jiayi Li – School of Materials Science and Engineering, Changchun University of Science and Technology, Changchun 130022, People's Republic of China
Binbin Xiao – School of Materials Science and Engineering, Changchun University of Science and Technology, Changchun 130022, People's Republic of China
Yiqing Wang – School of Materials Science and Engineering, Changchun University of Science and Technology, Changchun 130022, People's Republic of China

Complete contact information is available at:
<https://pubs.acs.org/10.1021/acsami.2c04369>

Notes

The authors declare no competing financial interest.

ACKNOWLEDGMENTS

The authors gratefully acknowledge the Project of College Students' Innovation and Entrepreneurship Training Program of Jilin Province (2021079) and the Jilin Province Scientific and Technological Development Program (20200201084JC) for support of this research.

REFERENCES

- (1) Qian, L.; Zheng, Y.; Xue, J. G.; Holloway, P. H. Stable and Efficient Quantum-Dot Light-Emitting Diodes Based on Solution-Processed Multilayer Structures. *Nat. Photonics* **2011**, *5*, S43–S48.
- (2) Song, J. J.; Wang, O. Y.; Shen, H. B.; Lin, Q. L.; Li, Z. H.; Wang, L.; Zhang, X. T.; Li, L. S. Over 30% External Quantum Efficiency Light-Emitting Diodes by Engineering Quantum Dot-Assisted Energy Level Match for Hole Transport Layer. *Adv. Funct. Mater.* **2019**, *29*, 1808377.
- (3) Lee, K.-H.; Han, C.-Y.; Kang, H.-D.; Ko, H.; Lee, C.; Lee, J.; Myoung, N. S.; Yim, S.-Y.; Yang, H. Highly Efficient, Color-Reproducible Full-Color Electroluminescent Devices Based on Red/Green/Blue Quantum Dot-Mixed Multilayer. *ACS Nano* **2015**, *9*, 10941–10949.
- (4) Li, X. Y.; Lin, Q. L.; Song, J. J.; Shen, H. B.; Zhang, H. M.; Li, L. S.; Li, X. G.; Du, Z. L. Quantum-Dot Light-Emitting Diodes for Outdoor Displays with High Stability at High Brightness. *Adv. Opt. Mater.* **2020**, *8*, 1901145.
- (5) Yang, J.; Choi, M. K.; Yang, U. J.; Kim, S. Y.; Kim, Y. S.; Kim, J. H.; Kim, D.-H.; Hyeon, T. Toward Full-Color Electroluminescent Quantum Dot Displays. *Nano Lett.* **2021**, *21* (1), 26–33.
- (6) Zhang, Y.; Cao, X. Electroluminescence of Green CdSe/ZnS Quantum Dots Enhanced by Harvesting Excitons from Phosphorescent Molecules. *Appl. Phys. Lett.* **2010**, *97*, 253115.
- (7) Cheng, Y.; Wan, H. Y.; Liang, T. Y.; Liu, C.; Wu, M. H.; Hong, H.; Liu, K. H.; Shen, H. B. Continuously Graded Quantum Dots: Synthesis, Applications in Quantum Dot Light-Emitting Diodes, and Perspectives. *J. Phys. Chem. Lett.* **2021**, *12* (25), 5967–5978.
- (8) Wang, F. Z.; Sun, W. D.; Liu, P.; Wang, Z. B.; Zhang, J.; Wei, J. L.; Li, Y.; Hayat, T.; Alsaedi, A.; Tan, Z. A. Achieving Balanced Charge Injection of Blue Quantum Dot Light-Emitting Diodes Through Transport Layer Doping Strategies. *J. Phys. Chem. Lett.* **2019**, *10*, 960–965.

- (9) Zhang, W. D.; Ding, S. H.; Zhuang, W. D.; Wu, D.; Liu, P.; Qu, X. W.; Liu, H. C.; Yang, H. C.; Wu, Z. H.; Wang, K.; Sun, X. W. InP/ZnS/ZnS core/shell Blue Quantum Dots for Efficient Light-Emitting Diodes. *Adv. Funct. Mater.* **2020**, *30*, 2005303.
- (10) Gao, M.; Yang, H. W.; Shen, H. B.; Zeng, Z. P.; Fan, F. J.; Tang, B. B.; Min, J. J.; Zhang, Y.; Hua, Q. Z.; Li, L. S.; Ji, B. T.; Du, Z. L. Bulk-like ZnSe Quantum Dots Enabling Efficient Ultrnarrow Blue Light-Emitting Diodes. *Nano Lett.* **2021**, *21*, 7252–7260.
- (11) Colvin, V. L.; Schlamp, M. C.; Alivisatos, A. P. Light-Emitting Diodes Made from Cadmium Selenide Nanocrystals and a Semiconducting Polymer. *Nature* **1994**, *370*, 354–357.
- (12) Woo, W.-K.; Shimizu, K. T.; Jarosz, M. V.; Neuhauser, R. G.; Leatherdale, C. A.; Rubner, M. A.; Bawendi, M. G. Reversible Charging of CdSe Nanocrystals in a Simple Solid-State Device. *Adv. Mater.* **2002**, *14*, 1068–1071.
- (13) Bae, W. K.; Park, Y.-S.; Lim, J.; Lee, D.; Padilha, L. A.; McDaniel, H.; Robel, I.; Lee, C.; Pietryga, J. M.; Klimov, Victor I. Controlling the influence of Auger recombination on the performance of quantum-dot light-emitting diodes. *Nat. Commun.* **2013**, *4*, 2661.
- (14) Bae, W. K.; Padilha, L. A.; Park, Y.-S.; McDaniel, H.; Robel, I.; Pietryga, J. M.; Klimov, V. I. Controlled Alloying of the Core–Shell Interface in CdSe/CdS Quantum Dots for Suppression of Auger Recombination. *ACS Nano* **2013**, *7*, 3411–3419.
- (15) Chang, J. H.; Park, P.; Jung, H.; Jeong, B. G.; Hahm, D.; Nagamine, G.; Ko, J.; Cho, J.; Padilha, L. A.; Lee, D. C.; Lee, C.; Char, K.; Bae, W. K. Unraveling the Origin of Operational Instability of Quantum Dot Based Light-Emitting Diodes. *ACS Nano* **2018**, *12*, 10231–10239.
- (16) Zhang, Y. Q.; Cao, X. A. Electroluminescence of Green CdSe/ZnS Quantum Dots Enhanced by Harvesting Excitons from Phosphorescent Molecules. *Appl. Phys. Lett.* **2010**, *97*, 253115.
- (17) Shirasaki, Y.; Supran, G. J.; Bawendi, M. G.; Bulović, V. Emergence of Colloidal Quantum-Dot Light-Emitting Technologies. *Nat. Photonics* **2013**, *7*, 13–23.
- (18) Angeloni, I.; Raja, W.; Brescia, R.; Polovitsyn, A.; De Donato, F.; Canepa, M.; Bertoni, G.; Proietti Zaccaria, R.; Moreels, I. Disentangling the Role of Shape, Ligands, and Dielectric Constants in the Absorption Properties of Colloidal CdSe/CdS Nanocrystals. *ACS Photonics* **2016**, *3*, 58–67.
- (19) Cho, I.; Jung, H.; Jeong, B. G.; Chang, J. H.; Kim, Y.; Char, K.; Lee, D. C.; Lee, C.; Cho, J.; Bae, W. K. Multifunctional Dendrimer Ligands for High-Efficiency, Solution-Processed Quantum Dot Light-Emitting Diodes. *ACS Nano* **2017**, *11*, 684–692.
- (20) Dai, X. L.; Zhang, Z. X.; Jin, Y. Z.; Niu, Y.; Cao, H. J.; Liang, X. Y.; Chen, L. W.; Wang, J. P.; Peng, X. G. Solution-Processed, High-Performance Light-Emitting Diodes based on Quantum Dots. *Nature* **2014**, *S15*, 96–99.
- (21) Zhang, H.; Sui, N.; Chi, X. C.; Wang, Y. H.; Liu, Q. H.; Zhang, H. Z.; Ji, W. Y. Ultrastable Quantum-Dot Light-Emitting Diodes by Suppression of Leakage Current and Exciton Quenching Processes. *ACS Appl. Mater. Interfaces* **2016**, *8*, 31385–31391.
- (22) Wang, H. C.; Zhang, H.; Chen, H. Y.; Yeh, H. C.; Tseng, M. R.; Chung, R. J.; Chen, S.; Liu, R. S. Cadmium-Free InP/ZnSeS/ZnS Heterostructure-Based Quantum Dot Light-Emitting Diodes with a ZnMgO Electron Transport Layer and a Brightness of Over 10000 cd m⁻². *Small* **2017**, *13*, 1603962.
- (23) Zhang, Z. X.; Ye, Y. X.; Pu, C. D.; Deng, Y. Z.; Dai, X. L.; Chen, X. P.; Chen, D.; Zheng, X. R.; Gao, Y.; Fang, W.; Peng, X. G.; Jin, Y. Z. High-Performance, Solution-Processed, and Insulating-Layer-Free Light-Emitting Diodes Based on Colloidal Quantum Dots. *Adv. Mater.* **2018**, *30*, 1801387.
- (24) Kim, H.-M.; Geng, D.; Kim, J.; Hwang, E.; Jang, J. Metal-Oxide Stacked Electron Transport Layer for Highly Efficient Inverted Quantum-Dot Light Emitting Diodes. *ACS Appl. Mater. Interfaces* **2016**, *8*, 28727–28736.
- (25) Kim, H.-M.; Cho, S.; Kim, J.; Shin, H.; Jang, J. Li and Mg Co-Doped Zinc Oxide Electron Transporting Layer for Highly Efficient Quantum Dot Light-Emitting Diodes. *ACS Appl. Mater. Interfaces* **2018**, *10*, 24028–24036.
- (26) Kim, D.; Fu, Y.; Kim, S.; Lee, W.; Lee, K.-H.; Chung, H. K.; Lee, H.-J.; Yang, H.; Chae, H. Polyethylenimine Ethoxylated-Mediated All-Solution-Processed High-Performance Flexible Inverted Quantum Dot-Light-Emitting Device. *ACS Nano* **2017**, *11*, 1982–1990.
- (27) Kim, O.-S.; Kang, B.-H.; Lee, J.-S.; Lee, S.-W.; Cha, S.-H.; Lee, J.-W.; Kim, S.-W.; Kim, S.-H.; Kang, S.-W. Efficient Quantum Dots Light-Emitting Devices Using Polyvinyl Pyrrolidone-Capped ZnO Nanoparticles with Enhanced Charge Transport. *IEEE Electron Device Lett.* **2016**, *37*, 1022–1024.
- (28) Kim, H. H.; Park, S.; Yi, Y.; Son, D. I.; Park, C.; Hwang, D. K.; Choi, W. K. Inverted Quantum Dot Light Emitting Diodes Using Polyethylenimine Ethoxylated Modified ZnO. *Sci. Rep.* **2015**, *5*, 8968.
- (29) Rhee, S.; Chang, J. H.; Hahm, D.; Jeong, B. G.; Kim, J.; Lee, H.; Lim, J.; Hwang, E.; Kwak, J.; Bae, W. K. Tailoring the Electronic Landscape of Quantum Dot Light-Emitting Diodes for High Brightness and Stable Operation. *ACS Nano* **2020**, *14* (12), 17496–17504.
- (30) Ho, M. D.; Kim, D.; Kim, N.; Cho, S. M.; Chae, H. Polymer and Small Molecule Mixture for Organic Hole Transport Layers in Quantum Dot Light-Emitting Diodes. *ACS Appl. Mater. Interfaces* **2013**, *5*, 12369–12374.
- (31) Yang, Y. X.; Zheng, Y.; Cao, W. R.; Titov, A.; Hyvonen, J.; Manders, J. R.; Xue, J. G.; Holloway, P. H.; Qian, L. High-Efficiency Light-Emitting Devices Based on Quantum Dots with Tailored Nanostructures. *Nat. Photonics* **2015**, *9*, 259–266.
- (32) Cao, W. R.; Xiang, C. Y.; Yang, Y. X.; Chen, Q.; Chen, L. W.; Yan, X. L.; Qian, L. Highly Stable QLEDs with Improved Hole Injection via Quantum Dot Structure Tailoring. *Nat. Commun.* **2018**, *9*, 2608.
- (33) Chen, H. T.; Ding, K.; Fan, L. W.; Liu, W.; Zhang, R.; Xiang, S. P.; Zhang, Q.; Wang, L. All-Solution-Processed Quantum Dot Light Emitting Diodes Based on Double Hole Transport Layers by Hot Spin-Coating with Highly Efficient and Low Turn-On Voltage. *ACS Appl. Mater. Interfaces* **2018**, *10*, 29076–29082.
- (34) Lan, L. H.; Liu, B. C.; Tao, H.; Zou, J. H.; Jiang, C. B.; Xu, M.; Wang, L.; Peng, J. B.; Cao, Y. Preparation of Efficient Quantum Dot Light-Emitting Diodes by Balancing Charge Injection and Sensitizing Emitting Layer with Phosphorescent Dye. *J. Mater. Chem. C* **2019**, *7*, 5755–5763.
- (35) Liu, Y.; Jiang, C. B.; Song, C.; Wang, J. H.; Mu, L.; He, Z. W.; Zhong, Z. J.; Cun, Y. K.; Mai, C. H.; Wang, J.; Peng, J. B.; Cao, Y. Highly Efficient All-Solution Processed Inverted Quantum Dots Based Light Emitting Diodes. *ACS Nano* **2018**, *12*, 1564–1570.
- (36) Jiang, C. B.; Zou, J. H.; Liu, Y.; Song, C.; He, Z. W.; Zhong, Z. J.; Wang, J.; Yip, H.-L.; Peng, J. B.; Cao, Y. Fully Solution-Processed Tandem White Quantum-Dot Light-Emitting Diode with an External Quantum Efficiency Exceeding 25%. *ACS Nano* **2018**, *12*, 6040–6049.
- (37) Ji, W. Y.; Lv, Y.; Jing, P. T.; Zhang, H.; Wang, J.; Zhang, H. Z.; Zhao, J. L. Highly Efficient and Low Turn-On Voltage Quantum Dot Light-Emitting Diodes by Using a Stepwise Hole-Transport Layer. *ACS Appl. Mater. Interfaces* **2015**, *7*, 15955–15960.
- (38) Wang, L.; Chen, T.; Lin, Q. L.; Shen, H. B.; Wang, A. Q.; Wang, H. Z.; Li, C. Y.; Li, L. S. High-Performance Azure Blue Quantum Dot Light-Emitting Diodes via Doping PVK in Emitting Layer. *Org. Electron.* **2016**, *37*, 280–286.
- (39) Sun, Y. Z.; Jiang, Y. B.; Sun, X. W.; Zhang, S. D.; Chen, S. M. Beyond OLED: Efficient Quantum Dot Light-Emitting Diodes for Display and Lighting Application. *Chem. Rec.* **2019**, *19*, 1729–1752.
- (40) Matsusue, N.; Suzuki, Y.; Naito, H. Charge Carrier Transport in Neat Thin Films of Phosphorescent Iridium Complexes. *Jpn. J. Appl. Phys.* **2005**, *44*, 3691–3694.
- (41) Shen, Q. B.; Hao, Y. L.; Ma, L. Y.; Wang, X. Y. Comparative Study of Red/Green/Blue Quantum-Dot Light-Emitting Diodes by Time-Resolved Transient Electroluminescence. *J. Phys. Chem. Lett.* **2021**, *12*, 7019–7025.
- (42) Pan, J. Y.; Chen, J.; Huang, Q. Q.; Khan, Q.; Liu, X.; Tao, Z.; Zhang, Z. C.; Lei, W.; Nathan, A. Size Tunable ZnO Nanoparticles to

Enhance Electron Injection in Solution Processed QLEDs. *ACS Photonics* **2016**, *3*, 215–222.

(43) Kern, R.; Sastrawan, R.; Ferber, J.; Stangl, R.; Luther, J. Modeling and Interpretation of Electrical Impedance Spectra of Dye Solar Cells Operated Under Open-Circuit Conditions. *Electrochim. Acta* **2002**, *47*, 4213–4225.

(44) Mora-Seró, I.; Bisquert, J.; Fabregat-Santiago, F.; García-Belmonte, G.; Zoppi, G.; Durose, K.; Proskuryakov, Y.; Oja, I.; Belaidi, A.; Dittrich, T.; Tena-Zaera, R.; Katty, A.; Lévy-Clément, C.; Barrio, V.; Irvine, S. J. C. Implications of The Negative Capacitance Observed at Forward Bias in Nanocomposite and Polycrystalline Solar Cells. *Nano Lett.* **2006**, *6*, 640–650.

(45) Yang, L. Q.; Li, X. F.; Yang, Q. Q.; Wang, S. M.; Tian, H. K.; Ding, J. Q.; Wang, L. X. High-Performance Red Quantum-Dot Light-Emitting Diodes Based on Organic Electron Transporting Layer. *Adv. Funct. Mater.* **2021**, *31*, 2007686.

(46) Suárez, B.; González-Pedro, V.; Ripolles, T. S.; Sánchez, R. S.; Otero, L. A.; Mora-Sero, I. Recombination Study of Combined Halides (Cl, Br, I) Perovskite Solar Cells. *J. Phys. Chem. Lett.* **2014**, *5*, 1628–1635.

(47) Li, B.; Fang, Y. F.; Bai, P. L.; Wang, Y. Q.; Li, J. Y.; Xiao, B. B.; Wang, Y. P. Effect of PVK mixed TAPC as Hole Transport Layers on device performance of Red Quantum-Dot Light-Emitting Diodes. *J. Lumin.* **2022**, *247*, 118871.

□ Recommended by ACS

High-Efficiency, Large-Area, Flexible Top-Emitting Quantum-Dot Light-Emitting Diode

Hongwei Yu, Wenfa Xie, et al.

AUGUST 10, 2022

ACS PHOTONICS

READ ▶

Improved Thermal Stability and Operational Lifetime of Blue Fluorescent Organic Light-Emitting Diodes by Using a Mixed-Electron Transporting Layer

Min Seok Ki, Keewook Paeng, et al.

AUGUST 01, 2022

ACS MATERIALS LETTERS

READ ▶

Noninvasive and Direct Patterning of High-Resolution Full-Color Quantum Dot Arrays by Programmed Microwetting

Kyeong Min Song, Yeon Sik Jung, et al.

SEPTEMBER 21, 2022

ACS NANO

READ ▶

Realization of Highly Efficient InGaN Green Light-Emitting Diodes with Laser-Annealed Multiple-Quantum Well Structures: Formation of Quantum Dot Structures

Xinwei Wang, Ning Zhang, et al.

SEPTEMBER 06, 2022

ACS APPLIED OPTICAL MATERIALS

READ ▶

Get More Suggestions >